Detrick, R., Honnorez, J., Bryan, W. B., Juteau, T., et al., 1990
Proceedings of the Ocean Drilling Program, Scientific Results, Vol. 106/109

3. PETROLOGY OF PERIDOTITES FROM HOLE 670A, LEG 109[1]

Toshitsugu Fujii[2]

ABSTRACT

Two types of serpentinized peridotites from Hole 670A of Leg 109 were studied in detail. A small piece of relatively unaltered sample, 109-670A-9R-1, #3 (22–24 cm), is olivine websterite characterized by aluminous chromian spinel with Cr/(Cr + Al) ratio of about 0.2. The other minerals have compositions essentially identical with those in more commonly observed serpentinized harzburgite like 109-670A-9R-01, #12 (94–97 cm). The occurrence of pyroxene-rich peridotite with normal harzburgite suggests that small scale heterogeneity in modal compositions exists in the upper mantle beneath the Mid-Atlantic Ridge. Low Cr/Al ratios of spinel and pyroxenes of those peridotites indicate that they are relatively less refractory among peridotites ever recovered from the oceanic region. Textures and the estimated equilibration temperatures indicate that peridotites recovered from Hole 670A are recrystallized and reequilibrated at subsolidus temperature.

The occurrence of serpentinized peridotites from the rift valley of the active mid-oceanic ridge may suggest that they represent direct exposure of upwelling mantle materials rather than serpentine diapirs.

INTRODUCTION

Variously serpentinized peridotites have been sampled by dredging and drilling in the oceanic region. These abyssal peridotites are generally interpreted as mantle fragments which are tectonically brought up to the surface by movements along transform faults (e.g., Melson and Thompson, 1971). The finding of serpentinized peridotites within a rift valley (Karson et al., 1986) remote from the Kane Fracture Zone, however, probably results in different interpretation of the mechanism of peridotite emplacement.

Also, most peridotites ever recovered are from fracture zones where present volcanic activities are lacking, and their relationships with the mantle materials beneath the active rift area, where accretion of oceanic crust is ongoing, are not clear. Those from Hole 670A are adequate samples for studying the nature of upper mantle beneath the oceanic ridge because they were recovered from rift valley and some of them preserve the original minerals.

In the present paper, we describe in detail two types of serpentinized peridotites recovered from Hole 670A and discuss the relationships between fracture zone and non-fracture zone peridotites.

PETROGRAPHIC DESCRIPTION

Among the ultramafic rocks recovered from Hole 670A, serpentinized harzburgites with porphyroclastic texture are most commonly observed and only one sample, 109-670A-9R-1, #3 (22–24 cm), shows somewhat different texture and quite different modal composition. Because of its peculiar modal characteristics, this sample was selected for detailed study. Another sample, 109-670A-9R-1, #12 (94–97 cm), was also studied as a representative of more commonly found serpentinized harzburgite at Hole 670A.

Sample 109-670A-9R-1, #3 (22–24 cm)

This sample is probably the least serpentinized sample among those recovered from Hole 670A and the degree of serpentinization is about 10% in total. Serpentinization is most intense at the margin of the recovered sample (about 3 cm across), and the degree of serpentinization at the interior is less than 5%. It is olivine websterite containing 60% of orthopyroxene, 20% of olivine, 20% of clinopyroxene, and less than 1% of chromian spinel.

Porphyroclasts are composed of both orthopyroxene (1–6 mm) and clinopyroxene (0.5–2 mm), and are surrounded by a matrix of polygonal olivine, clinopyroxene, and orthopyroxene whose sizes range from 0.1 to 0.4 mm (Fig. 1). Small chromian spinels (0.01–0.05 mm) are sparsely distributed among matrix minerals. Both orthopyroxene and clinopyroxene porphyroclasts contain thin exsolution lamellae ranging in thickness from submicrometers to 100 μm, and some of them show undulatory extinction and kink bands. Some of medium size matrix clinopyroxene (0.3–0.4 mm) also contain very thin lamellae of orthopyroxene and/or spinel, indicating that they could be dismembered fragments of clinopyroxene porphyroclast. Most of matrix pyroxenes less than 0.2 mm are clear and contain no exsolution lamellae.

Sample 109-670A-9R-1,#12 (94–97 cm)

This sample belongs to a common type of serpentinized clinopyroxene-bearing harzburgite recovered from Hole 670A and shows typical porphyroclastic texture. Olivine in this sample occurs as small fragments (0.02–0.3 mm) embedded in a matrix of mesh-textured serpentine. A group of isolated grains of olivine show similar interference colors and extinguish simultaneously under crossed polarized light, indicating that the original size of olivine grain before serpentinization was about 0.6–2 mm across. Orthopyroxenes are elliptical with size ranging from 0.8 to 6 mm. Clinopyroxene exsolution lamellae are observed in all the orthopyroxene grains. Some orthopyroxene porphyroclasts show undulatory extinction and gently bent cleavages. Clinopyroxenes also form porphyroclasts and have exsolution lamellae of orthopyroxene. Undulatory extinction and bent cleavages are also observed. Occasionally, small orthopyroxenes and clinopyroxenes (about 0.2 mm) are observed around porphyroclastic pyroxenes and some occur interstitially among olivines. Most spinels in this sample are oxidized to magnetite and those preserving original compositions are very rare.

[1] Detrick, R., Honnorez, J., Bryan, W. B., Juteau, T., et al., 1990. *Proc. ODP, Sci. Results*, 106/109: College Station, TX (Ocean Drilling Program).
[2] Earthquake Research Institute, University of Tokyo, Yayoi, Tokyo 113, Japan.

Degree of serpentinization of this sample is about 70% and even some pyroxene porphyroclasts are altered to bastite.

MINERAL CHEMISTRY

Mineral analyses were obtained at Geological Institute, University of Tokyo, using an electron-probe microanalyzer with the wave-length dispersive spectrometer JEOL JCMA-II. The beam current of 12 nA was maintained through the analysis. Correction procedures are based on the method by Bence and Albee (1968). Ferric iron content of spinel was calculated from charge balance consideration. Iron in other minerals was assumed as ferrous. Selected analyses of minerals are shown in Table 1 and 2.

Olivine

Mg# of olivine is within a narrow range of 90.4–91.4 in both samples, Sample 109-670A-9R-1, #3 (22–24 cm) and #12 (94–97 cm) (Fig. 2). No significant compositional zoning or grain-by-grain variation is detected. NiO contents are about 0.4 wt% and any systematic correlation with grain size is not detected.

Orthopyroxene

Microprobe analyses of large orthopyroxene grains with a focused electron beam (1–2 μm in diameter) sometimes resulted in some fluctuation in their Wo contents although we carefully avoided spots close to the optically visible clinopyroxene lamellae (Fig. 3A). This is because orthopyroxene contains very thin clinopyroxene lamellae ranging in thickness from submicrometers to several tens of micrometers with spacing of one to several tens of micrometers. On the contrary, small polygonal orthopyroxene grains in the matrix and relatively thick lamellae (about 20 μm in thickness) within large clinopyroxene grains show almost constantly low Wo contents, and they are almost identical to the composition of the spots within a large orthopyroxene grain, where no clinopyroxene lamellae are observed even with back-scattering electron image (BEI) of scanning electron microscope (SEM). In order to obtain the bulk compositions of orthopyroxene, several areas of 50 × 50 μm within a porphyroclast were analyzed with scanning beam and they were averaged. The compositions so obtained are almost uniform within a given specimen.

Mg# and Wo contents of orthopyroxenes are almost identical in both samples, 109-670A-9R-1, #3 (22–24 cm), and #12 (94–97 cm) (Fig. 3A). Cr_2O_3/Al_2O_3 ratio of orthopyroxene in 109-670A-9R-1, #3 (22–24 cm), is less than that in #12 (94–97 cm) (Fig. 4A), probably reflecting the composition of coexisting spinel: spinels in 109-670A-9R-1, #3 (22–24 cm), are more aluminous than in #12 (94–97 cm).

Clinopyroxene

Microprobe analyses of large clinopyroxene grains also resulted in some fluctuation of Wo contents because of the existence of very thin lamellae of orthopyroxene (Fig. 3B). Small polygonal clinopyroxene in the matrix and relatively thick clinopyroxene lamellae within orthopyroxene show almost constant composition and are high in Wo content (about 47 mole%). Attempt to obtain the bulk compositions of several large clinopyroxene porphyroclasts also resulted in a uniform composition. Cr_2O_3/Al_2O_3 ratio is higher in clinopyroxenes of 109-670A-9R-1, #12 (94–97 cm), than those of #3 (22–24 cm) although the ranges of Al_2O_3 contents are identical (Fig. 4B).

Spinel

Brown spinels have compositions relatively rich in Al_2O_3 among those within abyssal peridotites (e.g., Dick and Bullen,

A

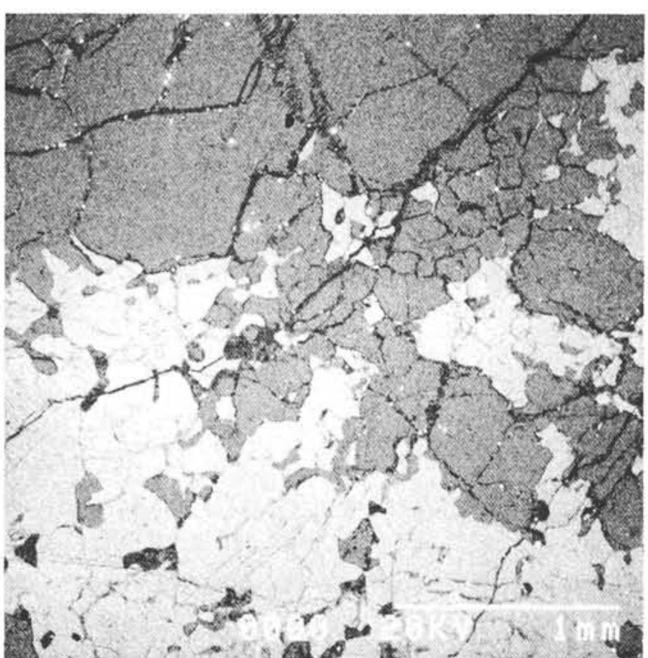

B

Figure 1. Texture of Leg 109 peridotite (109-670A-9R-1, #3 (22–24 cm)). **A.** Photomicrograph in ordinary light. **B.** BEI (Back-scattering Electron Image) of the same area. Dark colored mineral is orthopyroxene and light colored minerals are clinopyroxene and olivine. Note the differences in grain size between porphyroclasts and matrix polygonal minerals.

Table 1. Selected analyses of minerals of 109-670A-9R-1, piece 3 (20–22 cm).

No. Sample ID	1 OLV L-1	2 OLV S-1	3 OPX S-1	4 OPX L-1	5 CPX S-1	6 CPX L-1	7 SPN 1-1	8 SPN 2-1
SiO_2	40.66	40.60	54.52	54.53	50.97	51.99	0.11	0.10
Al_2O_3	0.01	0.02	4.34	3.82	5.34	5.41	50.44	48.20
TiO_2	0.00	0.00	0.04	0.06	0.12	0.12	0.05	0.00
Cr_2O_3	0.00	0.00	0.66	0.52	0.99	0.99	17.14	18.57
Fe_2O_3	0.00	0.00	0.00	0.00	0.00	0.00	0.85	2.17
FeO	8.96	9.15	5.81	5.75	2.63	3.32	12.81	12.32
MnO	0.08	0.12	0.13	0.12	0.08	0.08	0.15	0.07
MgO	49.77	50.23	33.21	31.91	16.50	19.03	17.29	17.32
CaO	0.04	0.03	1.05	2.69	22.62	19.25	0.01	0.09
Na_2O	0.00	0.00	0.00	0.00	0.14	0.14	0.00	0.00
NiO	0.45	0.43	0.10	0.08	0.05	0.10	0.39	0.39
V2O3	0.00	0.00	0.03	0.05	0.05	0.02	0.10	0.05
Total	99.96	100.57	99.88	99.54	99.48	100.45	99.34	99.26
Oxygen	4.000	4.000	6.000	6.000	6.000	6.000	4.000	4.000
Si	0.995	0.989	1.888	1.902	1.864	1.868	0.003	0.003
Al	0.000	0.001	0.177	0.157	0.230	0.229	1.609	1.551
Ti	0.000	0.000	0.001	0.002	0.003	0.003	0.001	0.000
Cr	0.000	0.000	0.018	0.000	0.000	0.028	0.367	0.401
Fe^{3+}	0.000	0.000	0.000	0.000	0.000	0.000	0.017	0.045
Fe^{2+}	0.183	0.186	0.168	0.168	0.080	0.100	0.290	0.281
Mn	0.002	0.003	0.004	0.004	0.002	0.002	0.003	0.002
Mg	1.815	1.824	1.714	1.659	0.900	1.019	0.698	0.705
Ca	0.001	0.001	0.039	0.100	0.886	0.741	0.000	0.002
Na	0.000	0.000	0.000	0.000	0.010	0.009	0.000	0.000
Ni	0.009	0.008	0.003	0.002	0.001	0.003	0.009	0.009
V	0.000	0.000	0.001	0.001	0.001	0.001	0.002	0.001
Sum	3.005	3.011	4.013	4.010	4.008	4.004	2.999	2.999
Ratio								
Mg/Mg + Fe	90.8	90.7	91.1	90.8	91.8	91.1	70.6	71.5
Wo(Al)	–	–	2.0	5.2	47.5	39.8	80.7	77.7
En(Cr)	–	–	89.2	86.1	48.2	54.8	18.4	20.1
Fs(Fe^{3+})	–	–	8.8	8.7	4.3	5.4	0.9	2.2

1. OLV L-1 = Large olivine.
2. OLV S-1 = Small olivine in matrix.
3. OPX S-1 = Small orthopyroxene (0.1 mm) in matrix.
4. OPX L-1 = Porphyroclastic orthopyroxene, averaged bulk composition.
5. CPX S-1 = Small clinopyroxene (0.2 mm) in matrix.
6. CPX L-1 = Porphyroclastic clinopyroxene, averaged bulk composition.
7. SPN 1-1 = Spinel in matrix contacting with olv and cpx, core.
8. SPN 2-1 = Spinel in serpentinized matrix, core.

1984) and similar to those from spinel lherzolite nodule (e.g., Ozawa, 1986). The Cr/(Cr + Al) and Mg/(Mg + Fe^{2+}) ratios of spinels in 109-670A-9R-1, #3 (22–24 cm), range from 0.17 to 0.21 and from 0.72 to 0.68, respectively (Fig. 5). Only one analysis of spinel is available for #12 (94–97 cm), and it is more chromian (Cr/(Cr + Al) = 0.31 and Mg/(Mg + Fe^{2+}) = 0.68 than those in 109-670A-9R-1, #3 (22–24 cm).

COMPARISON WITH PERIDOTITES FROM LEG 45

During Leg 45, serpentinized spinel harzburgite and lherzolite were recovered from Holes 395 and 395A, about 100 km west of Hole 670A (Melson, Rabinowitz, et al., 1978) and almost on the identical latitude. Those peridotites are sandwiched between pillow lava sequences, and they could have been exposed at the rift valley like peridotites of Leg 109 and they were covered by basalt lavas of later volcanic activity. The comparison of the petrographical characteristics of peridotites from those two legs, therefore, might be significant in understanding temporal variation of the upper mantle beneath the Mid-Atlantic Ridge, if any, and in understanding the possible mineralogical variations of the upper mantle within the same oceanic plate segment. Arai and Fujii (1978) and Sinton (1978) described the peridotites from Leg 45. Although they have published detailed analyses of constituting minerals, we have attempted to re-analyze with the same procedure we described above in order to make the comparison more precisely.

The textures of the Leg 45 peridotites are similar to those of the common type of Leg 109 peridotites, serpentinized harzburgite with porphyroclastic texture; however, the mineral chemistry is somewhat different. Most obvious difference is observed in the compositions of spinels. Spinels of Leg 45 peridotites are much more chromian (Cr/(Cr + Al) = 0.35–0.42) than those of Leg 109 peridotite (Fig. 5). Composition of pyroxenes is also slightly different; less aluminous and more chromian in Leg 45 peridotites (Fig. 4). Composition of olivine is almost identical in peridotites of both legs although olivine from Leg 45, 18-1, #2C shows wider range of Fo content (Fig. 2).

Considering that Leg 109 peridotites contain more aluminous pyroxenes and spinels than Leg 45 peridotites, the former peridotites might be slightly less refractory than the latter. The difference is, however, only subtle and is within a

Table 2. Selected analyses of minerals of 109-670A-9R-1, piece 12 (94–97 cm).

No. Sample ID	1 OLV L-1	2 OPX L-1	3 OPX L-2	4 OPX S-1	5 CPX L-1	6 CPX L-2	7 SPN 1-1
SiO_2	40.24	54.24	54.84	55.44	50.71	51.08	0.06
Al_2O_3	0.00	4.09	3.48	2.48	5.55	5.27	40.82
TiO_2	0.00	0.00	0.09	0.03	0.14	0.08	0.02
Cr_2O_3	0.03	0.98	0.79	0.53	1.56	1.44	27.13
Fe_2O_3	0.00	0.00	0.00	0.00	0.00	0.00	1.39
FeO	9.04	5.72	5.75	5.66	2.68	3.21	13.27
MnO	0.13	0.14	0.18	0.14	0.07	0.09	0.19
MgO	49.42	31.57	33.45	34.29	16.14	19.30	16.07
CaO	0.04	2.79	1.30	0.81	22.85	18.62	0.02
Na_2O	0.00	0.00	0.00	0.00	0.26	0.24	0.00
NiO	0.37	0.12	0.13	0.14	0.07	0.17	0.20
V_2O_3	0.00	0.07	0.00	0.05	0.03	0.04	0.14
Total	99.27	99.71	100.01	99.56	100.05	99.53	99.31
Oxygen	4.000	6.000	6.00	6.000	6.000	6.000	4.000
Si	0.992	1.892	1.900	1.924	1.850	1.855	0.002
Al	0.000	0.168	0.142	0.101	0.238	0.225	1.359
Ti	0.000	0.000	0.002	0.001	0.004	0.002	0.000
Cr	0.001	0.027	0.022	0.014	0.045	0.041	0.606
Fe^{3+}	0.000	0.000	0.000	0.000	0.000	0.000	0.030
Fe^{2+}	0.186	0.167	0.166	0.164	0.082	0.097	0.313
Mn	0.003	0.004	0.005	0.004	0.002	0.003	0.005
Mg	1.817	1.642	1.727	1.773	0.878	1.045	0.677
Ca	0.001	0.104	0.048	0.030	0.893	0.725	0.001
Na	0.000	0.000	0.000	0.000	0.018	0.017	0.000
Ni	0.007	0.003	0.004	0.004	0.002	0.005	0.005
V	0.000	0.002	0.000	0.001	0.001	0.001	0.003
Sum	3.007	4.009	4.016	4.017	4.013	4.017	2.999
Ratio							
Mg/Mg + Fe	90.7	90.8	91.2	91.5	91.5	91.5	68.3
Wo(Al)	–	5.4	2.5	1.5	48.2	38.8	68.1
En(Cr)	–	85.8	88.9	90.1	47.4	56.0	30.4
Fs(Fe^{3+})	–	8.7	8.6	8.3	4.4	5.2	1.5

1. OLV L-1 = Isolated olivine grain within serpentine mesh structure.
2. OPX L-1 = Porphyroclastic orthopyroxene, averaged bulk composition.
3. OPX L-2 = Porphyroclastic orthopyroxene, lamellae-free portion.
4. OPX S-1 = Small grain beside porphyroclastic orthopyroxene.
5. CPX L-1 = Porphyroclastic clinopyroxene, lamellae-free portion.
6. CPX L-2 = Porphyroclastic clinopyroxene, averaged bulk composition.
7. SPN 1-1 = Spinel within serpentine matrix.

variation of abyssal peridotites from Atlantic region (e.g., Michael and Bonatti, 1985).

ESTIMATION OF EQUILIBRATION TEMPERATURE

Many geothermometers have been proposed for estimation of the equilibration temperatures of ultramafic rocks; however, there is not any clear criterion to decide which one gives reliable value. We adopted the thermometer of Wells (1977) simply because that seems to be most commonly used (Fujii and Scarfe, 1982). The estimated temperatures for pairs of polygonal small pyroxenes in the matrix and for pairs of exsolution lamellae and their host pyroxenes are the lowest, and they are around 1000°C. When the thermometer is applied to the pair of averaged compositions of large pyroxenes, estimated equilibrium temperatures are within a range of 1200–1250°C, which may be close to the temperature of igneous event.

Application of the olivine-spinel geothermometer (Fabries, 1979) to the Leg 109 peridotites results in quite low temperature around 650°C. It could be possible that the sample was finally equilibrated at such low temperature and that the estimated temperature based on two-pyroxene thermometer may indicate the closing temperature for Ca diffusion in pyroxenes. It should be noted, however, that the enthalpy change of Fe-Mg exchange reaction between olivine and aluminous spinel is very small, and consequently the thermometer for spinels with Cr/(Cr + Al) ratio less than 0.2 is not accurate.

DISCUSSION

One of the samples described in this report (109-670A-9R-1, #3 (22–24 cm)) shows quite different modal compositions from more commonly found abyssal peridotite. Similarities in mineral compositions and in porphyroclastic texture with usual serpentinized peridotites suggest, however, the sample was derived from the upper mantle like other abyssal peridotites. It is probable that small-scale heterogeneity in mineral proportion exists in the upper mantle beneath rift valley.

Michael and Bonatti (1985) discussed that fracture zone peridotites are slightly less refractory than non-fracture zone peridotites in the region of the Kane and the Atlantic Fracture Zones. Their arguments are based on the study of Leg 45

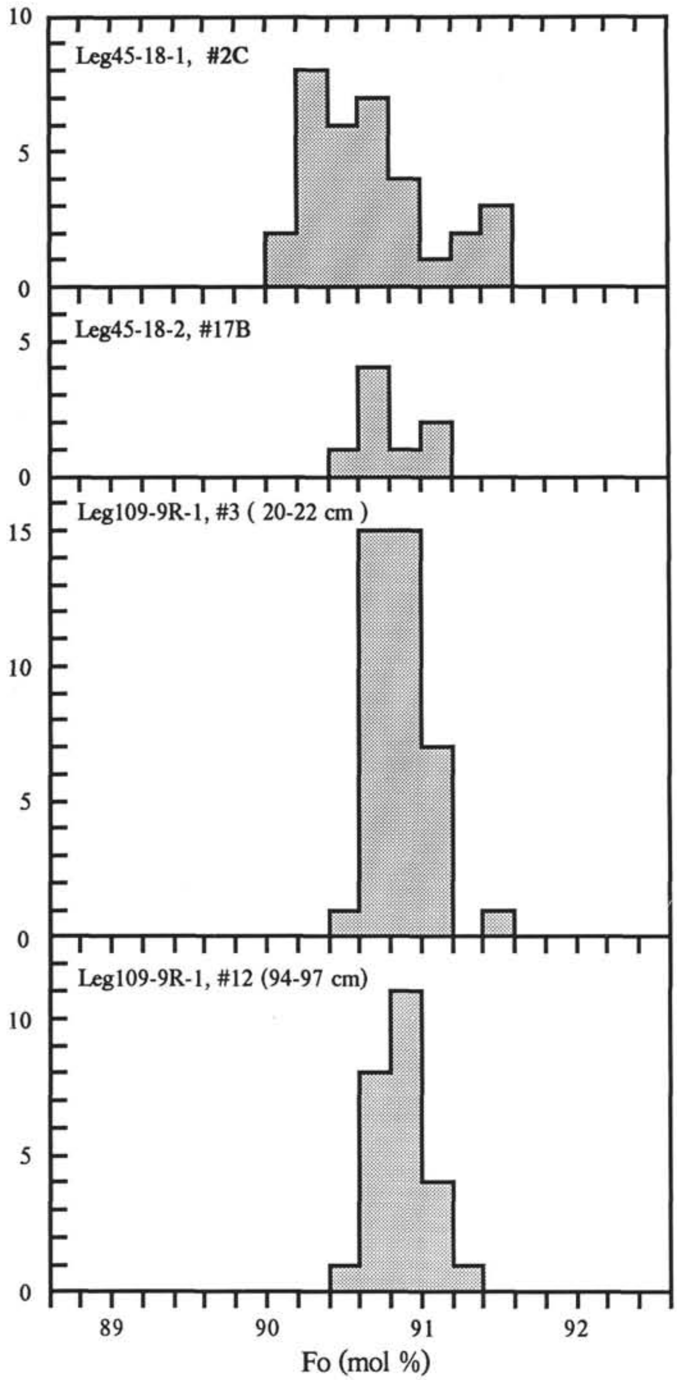

Figure 2. Histograms showing olivine composition (Fo content).

peridotites (Site 395) as a representative of non-fracture zone peridotites. As described above, the Leg 109 peridotites are less refractory than the Leg 45 peridotites and also seem to be less refractory than the Kane Fracture Zone and the Atlantic Fracture Zone peridotites considering the Cr/(Cr + Al) ratios in spinel and the Cr/Al ratios in pyroxenes. It is probable, therefore, that there is no significant difference between fracture zone and non-fracture zone peridotites and that fracture zone peridotites could be generally representative of the peridotites for a given region.

When peridotites were recovered from the normal oceanic floor remote from any fracture zone during Leg 45, Arai and Fujii (1978) discussed that, because those peridotites are covered by pillow lava sequence, they must have once exposed within the rift axis of the Mid-Atlantic ridge. The recovery of serpentinized peridotites from Leg 109 indicates that the process is not rare at the Mid-Atlantic ridge.

As discussed in Detrick, Honnorez, Bryan, Juteau, et al. (1988), two possible models could be considered as for the mode of emplacement of these serpentinized peridotite. One model assumes that the upper mantle peridotites were serpentinized by penetration of seawater along normal faults within rift valley and obtained buoyancy due to volume expansion. Because of this buoyancy, serpentinized peridotites might ascend to the surface along faults as serpentine diapirs. The other model is that mantle materials could be exposed on the surface when volcanic activity at rift axis is in rest and spreading of ocean floor is continuing, because any accretion of basaltic crust covering the mantle materials is not made.

Our favorite model is that those peridotites represent direct exposure of upwelling mantle materials because igneous activity at a slow spreading ridge is probably intermittent, and consequently formation of basaltic crust might fail at some time intervals. This model seems to be reasonable because we do not need to expect extraordinary low temperature at the upper mantle beneath axial rift area; on the contrary, serpentine diapir model requires low temperature (less than 500°C) at the upper mantle for peridotite to be serpentinized before getting buoyancy within oceanic crust.

REFERENCES

Arai, S., and Fujii, T., 1978. Petrology of ultramafic rocks from site 395. *In* Melson, W. G., Rabinowitz, P. D., et al., *Init. Repts. DSDP,* 45: Washington (U.S. Govt. Printing Office), 587–594.

Bence, A. E., and Albee, A. L., 1968. Empirical correction factors for the electron microanalysis of silicate and oxides. *J. Geol.,* 76:382–403.

Detrick, R., Honnorez, J., Bryan, W. B., Thierry, J., et al., 1988. *Proc. ODP, Init. Repts.,* 106/109: College Station, TX (Ocean Drilling Program).

Dick, H.J.B., and Bullen, T., 1984. Chromian spinel as a petrogenetic indicator in abyssal and alpine-type peridotites and spatially associated lavas. *Contrib. Mineral. Petrol.,* 86:54–76.

Fabries, J., 1980 . Spinel-olivine geothermometry in peridotites from ultramafic complexes. *Contrib. Mineral. Petrol.,* 69:329–336.

Fujii, T., and Scarfe, C. M., 1982. Petrology of ultramafic nodules from West Kettle River near Kelowna, Southern British Columbia. *Contrib. Mineral. Petrol.,* 80:297–306.

Karson, J. A., Brown, J. R., and Winters, A. T., 1986. Seafloor spreading in the MARK area. *EOS,* 67:1213.

Melson, W. G., and Thompson, G., 1971. Petrology of a transform fault zone and adjacent ridge segments. *Phil. Trans. R. Soc. London,* 268:423–441.

Melson, W. G., Rabinowitz, P. D., et al., 1978. *Init. Repts. DSDP,* 45: Washington (U.S. Govt. Printing Office).

Michael, P. J., and Bonatti, E., 1985. Peridotite composition from the North Atlantic: regional and tectonic variations and implications for partial melting. *Earth Planet. Sci. Lett.,* 73:91–104.

Ozawa, K., 1986. Partitioning of elements between constituent minerals in peridotites from the Miyamori ultramafic complex, Kitakami Mountains, northeast Japan: Estimation of P-T condition and igneous composition of minerals. *J. Fac. Sci., Univ. Tokyo,* 21:115–137.

Sinton, J. M., 1978. Petrology of (alpine type) peridotites from Site 395, DSDP Leg 45, *In* Melson, W. G., Rabinowitz, P. D., et al., *Init. Repts. DSDP,* 45: Washington (U.S. Govt. Printing Office), 595–601.

Wells, P.R.A., 1979. Pyroxene thermometry in simple and complex systems. *Contrib. Mineral. Petrol.,* 62:129–139.

Date of initial receipt: 31 August 1988
Date of acceptance: 20 April 1989
Ms 106/109B-116

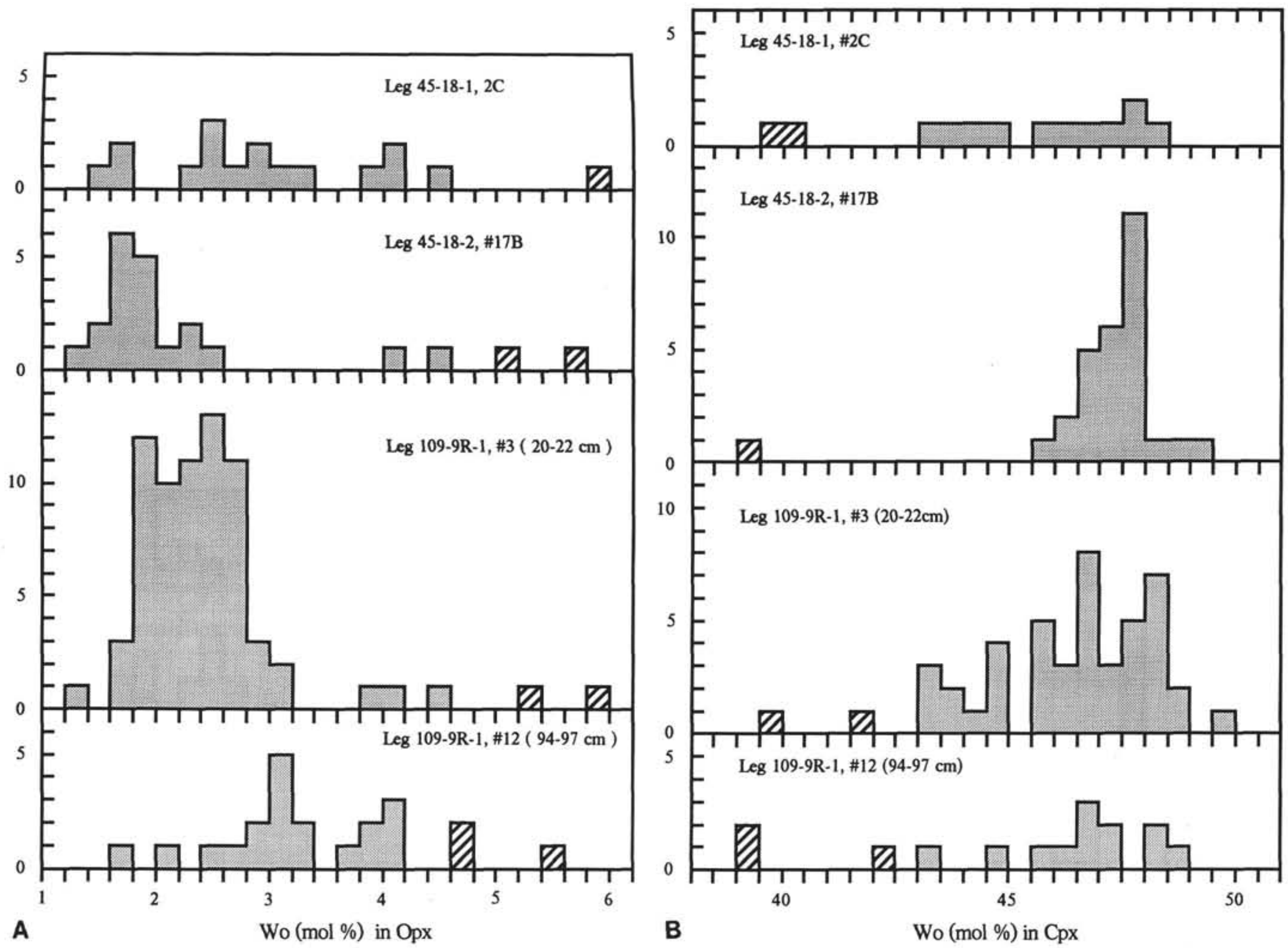

Figure 3. Histograms showing pyroxene compositions (Wo content). **A.** Orthopyroxene. **B.** Clinopyroxene. Hatched block indicates the averaged composition obtained by scanning analysis over a certain extent of area of pyroxenes with thin exsolution lamellae.

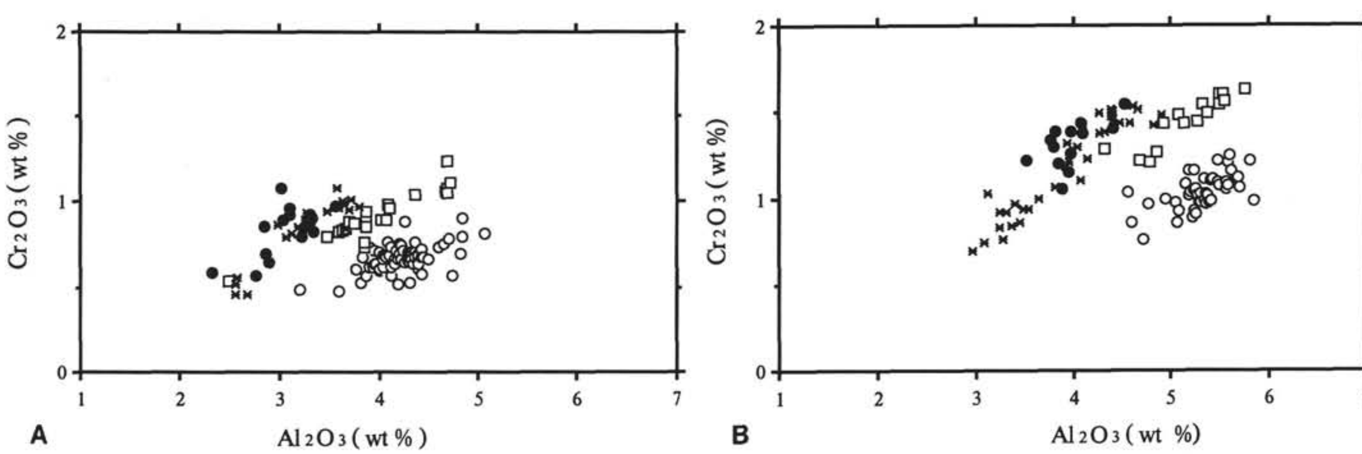

Figure 4. Al_2O_3 vs. Cr_2O_3 (wt%) for pyroxenes. **A.** Orthopyroxene. **B.** Clinopyroxene. Open circle = 109-670A-9R-1, #3 (22–24 cm); open square = 109-670A-9R-1, #12 (94–97 cm); solid circle = Leg 45-395, 18-1, #2C; asterisk = Leg 45-395, 18-2, #17B.

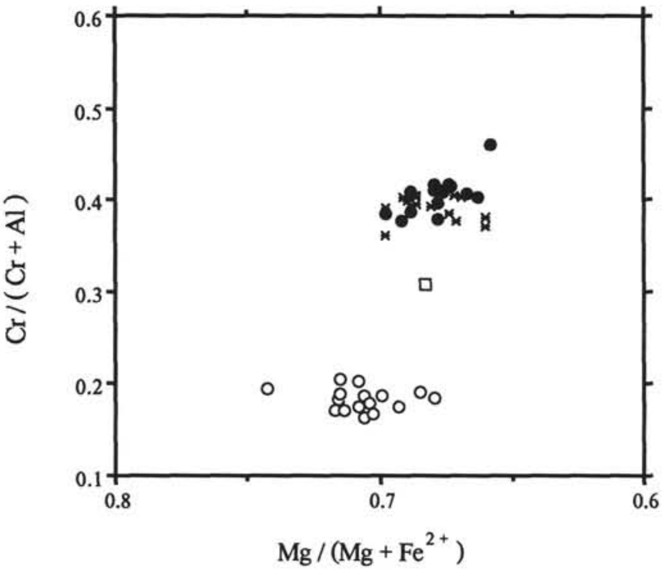

Figure 5. Mg# vs. Cr/(Cr + Al) for spinels. Symbols as in Figure 4.